Origin of Activation Barriers in the Dimerization of Neutral Radicals: A "Nonperfect Synchronization" Effect?

Cyrille Costentin and Jean-Michel Savéant*

Laboratoire d'Electrochimie Moléculaire, Unité Mixte de Recherche Université - CNRS No. 7591, Université de Paris 7 - Denis Diderot, 2 place Jussieu, 75251 Paris Cedex 05, France

Received: January 3, 2005; In Final Form: March 7, 2005

Dimerizations of delocalized neutral radicals may be endowed with quite significant activation barriers. The origin of these barriers is discussed in terms of a model that emphasizes the role of localization of the unpaired radical upon bond formation. Several examples are given in which the model is compared with the results of quantum chemical calculations including the coupling of allyl radicals and of benzyl radicals at various possible carbon sites. The dimerization behavior of radicals in the NADH family is also examined. The connection between the reasons that underlay the existence of the activation barrier and the principle of "nonperfect synchronization" is discussed. The dimerization of conjugated radicals indeed offers a precious example that can be used to decipher the reasons behind these behaviors, being devoid of the ambiguities arising from the simultaneous involvement of ionic and covalent states, significant solvent reorganization, and the contribution of extensive proton tunneling, in the mostly discussed case of proton transfer at carbon.

Introduction

Neutral carbon-centered radicals are classically categorized according to their "persistency" and their "stabilization".[1] Stabilization is defined on the basis of H-atom exchange, taking alkanes as references. It may be alternatively gauged after rotation decoupling of electron delocalization. Persistency appears to be essentially related to steric hindrance and typically concerns dimerization reactions. In the absence of steric hindrance, dimerization is reputed not to involve an activation barrier, the potential energy profiles being described by Morse curves with a good approximation. This behavior, or assumed behavior, forms the basis of determinations of bond dissociation energies by kinetic techniques,[2] as, for example, flash pyrolysis.[3] In the course of an investigation of the factors that govern the enthalpic and entropic characteristics of ion radical dimerizations,[4] we were led to compare them with their protonated analogues. We then found many examples where the coupling reaction of these neutral radicals is endowed with a significant activation barrier in the case where the unpaired electron is delocalized over the whole molecule rather than confined on the dimerizing carbon center. The description of such cases in the literature is very scarce,[5,6] even if the effect of the reversibility of certain dimerization reactions on the overall kinetics has been mentioned.[7]

In the following discussion, after a general presentation of several examples, where quantum chemical calculations reveal the existence of significant activation barriers, their origin will be discussed in the framework of a two-state model based on the combination of a bonding state and a nonbonding state. Ways of approximating the potential energy profiles of these states and the resonance energy for their mixing will then be delineated and applied to several examples. The next and last question that we will address is the possible relationship between the reasons, thus uncovered, that underlay the existence and magnitude of the activation barrier on the one hand and the notion of the "nonperfect synchronization" of events in the course of a chemical reaction on the other. This notion has been mostly illustrated by protonation/deprotonation at carbon atoms.[8] The dimerization of neutral radicals is an attractive example for undertaking such a discussion, because unlike protonation/deprotonation reactions the problem is not obscured by complicating factors such as strong quantum effects (leading to extensive proton tunneling), mixing of homolytic and ionic states, and significant solvent reorganization.

In other words, we are not looking for an accurate calculation of small activation barriers but rather wish to uncover the key reasons behind the existence of substantial activation barriers for the dimerization of certain conjugated radicals as well as the absence of significant activation barriers for the dimerization of others.

Activation Barriers in the Coupling of Carbon-Centered Neutral Radicals

Figure 1 shows the potential energy profiles for the dimerization of a series of delocalized radicals exhibiting a significant activation barrier. At this first stage, calculations were restricted to the semiempirical level to multiply the examples. More elaborate calculations will be carried out further on when quantitative relationships will be sought. The formation of ethane from methyl radicals, also represented in Figure 1, serves as a reference system where there is no barrier and where the potential energy profile may be closely approximated by a Morse curve. Dimerization at the nonconjugated carbon of the butenyl radical shows, as expected, the same absence of activation barrier as in the methyl case. Activation barriers appear with conjugated radicals. As a general trend, they are larger when the unpaired electron density on the dimerizing carbon is smaller. In parallel, the dimerization activation energy increases as the thermodynamic driving force for forming the dimer decreases, the largest values being found for uphill dimerizations. However, substantial activation energies may be found even if dimerization is downhill. For example, the barrier, if

* Corresponding author. E-mail: saveant@paris7.jussieu.fr.

10.1021/jp050017+ CCC: $30.25
Published on Web 04/20/2005

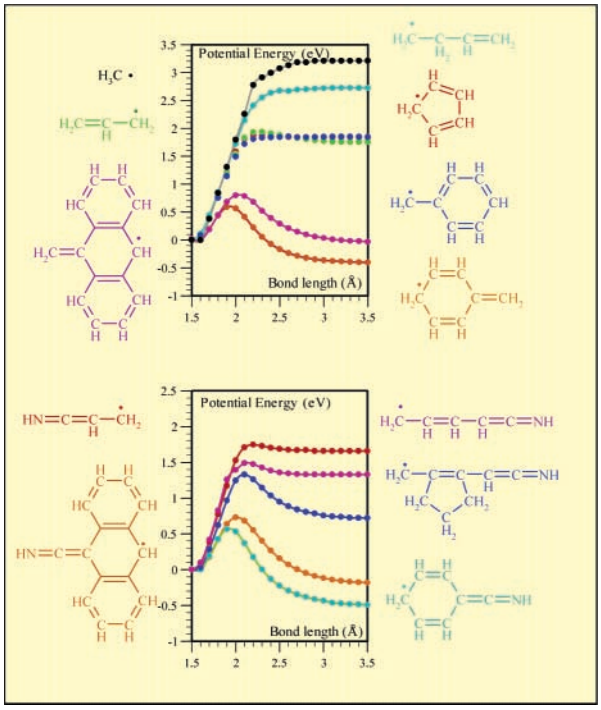

Figure 1. Potential energy profiles for a series of neutral carbon-centered radicals derived from AM1 calculations.

any, is very small, and the driving force is large for allyl, cyclopentadienyl, and benzyl. Dimerization in the para position of benzyl is both slightly uphill and endowed with a very large activation barrier. The same is true, albeit to a lesser extent for the anthracenyl analogue. The presence of an imino group increases delocalization, giving rise to several examples of significant activation energies even in cases where dimerization is downhill.

Design of a Two-State Model

From the dimer to the radicals, the hybridization of the dimerizing carbon passes from sp^3 to sp^2 as the bond stretches and breaks. However, this may not cause the existence of the activation barrier because the changes in angles and length are concomitant, participating both for the normal mode that leads to bond cleavage. A perusal of the examples given in Figure 1 strongly suggests that the origin of the activation barrier derives, when starting from the radicals, from a compromise between a gain in energy arising from the formation of the σ-bond on one hand and a loss in energy required by the localization of the unpaired electron on the dimerizing carbon on the other hand. The latter factor gets larger and larger as the unpaired electron is more and more delocalized over other sites of the molecule. The goal of the model described below is twofold: (i) to understand the origin of the activation barrier, if any and (ii) to predict the height of the barrier using only information relative to reactants and products.

Consider, for example, what happens in a simple case such as the dimerization of two allyl radicals. The allyl radical may be described by two mesomeric forms of equal weight in which the unpaired electron is localized at one end of the molecular framework. The actual radical is obtained by mixing these two forms labeled *A* and *B* (whose wave functions are Rumer functions as detailed in the Supporting Information) as shown at the top of Figure 2, with a gain in energy equal to the resonance energy, *H*.

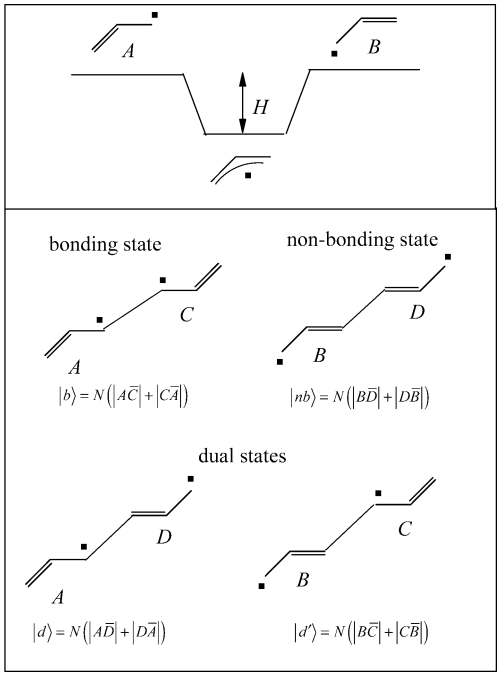

Figure 2. (Top) allyl radical. (Bottom) dimerization of allyl radicals; bonding, nonbonding, and dual states.

When two allyl radicals, described by forms *A*, *B* and *C*, *D*, respectively, get close to each other, four interactions have to be considered. Among them, only one may be called a bonding interaction because it involves mesomeric forms (*A* and *C*) in which an unpaired electron is localized at the end of each radical in a configuration where the two orbitals containing the unpaired electrons can mixed so as to form the dimer σ-bond when the distance between the ending carbons decreases. All other interactions are repulsive. They may be classified as nonbonding when it involves a two-bond repulsion through two mesomeric forms approaching each other from the side opposite the carbon bearing the unpaired electron (*B* and *D*) or dual when it involves a three-electron repulsion between an unpaired electron and a bond (i.e., *A* and *D* or *B* and *C*). In valence bond terms, this means that four valence bond states have to be considered to describe the adiabatic ground state. The corresponding valence bond wave functions may be described by a covalent valence bond structure $|b\rangle = N(|A\bar{C}| + |C\bar{A}|)$ (N is a normalization factor), a nonbonding valence bond structure $|nb\rangle = N(|B\bar{D}| + |D\bar{B}|)$, and two dual states $|d\rangle = N(|A\bar{D}| + |D\bar{A}|)$ and $|d'\rangle = N(|B\bar{C}| + |C\bar{B}|)$ (bottom of Figure 2). The adiabatic ground-state wave function ψ is thus a linear combination of these four valence bond states:

$$\psi = c_b|b\rangle + c_d|d\rangle + c_{d'}|d'\rangle + c_{nb}|nb\rangle$$

Because states $|d\rangle$, $|d'\rangle$, and $|nb\rangle$ correspond to repulsive states, ψ may be viewed as a combination of two states

$$\psi = c_b\Phi_b + c_{rep}\Phi_{rep}$$

where Φ_b is the covalent valence bond structure (noted $|b\rangle$ above) and Φ_{rep} a repulsive state that is not a pure diabatic valence bond state. This two-state description of radical dimerization thus requires the following steps: building the repulsive state, specifying the way in which the respective energy of each state varies with distance, and mixing of the bonding and repulsive states to finally obtain the adiabatic ground-state profile

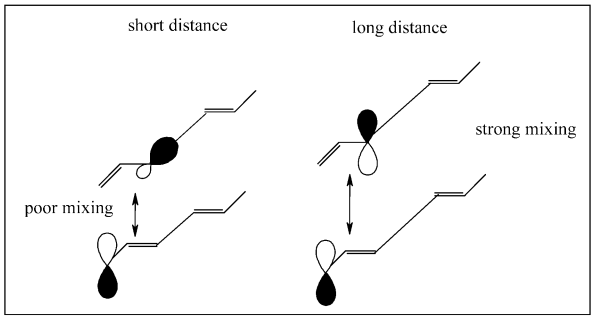

Figure 3. Dimerization of allyl radicals. Mixing of the mesomeric forms of an allyl radical at short and long dimerization distances. Example of mixing of a dual state with the nonbonding state.

from which the location of the transition state and the activation energy derive.

Building of the repulsive states is as follows. The combination of the three valence bond states $|d\rangle$, $|d'\rangle$, and $|nb\rangle$ leads to three repulsive states Φ^i_{rep} ($i = 1$, 2, or 3). Φ_{rep} is a combination of the three states Φ^i_{rep}. Because we are interested only in the adiabatic ground state, we assume that ψ may be considered to be a mixture of the more stable repulsive state, labeled Φ^1_{rep}, with the bonding state:

$$\psi = c_b\Phi_b + c_{\text{rep}}\Phi_{\text{rep}} \approx c_b\Phi_b + c^1_{\text{rep}}\,\Phi^1_{\text{rep}}$$

We are thus lead to the determination of energy profile $E_\Phi(r)$ corresponding to the more stable repulsive state Φ^1_{rep} through the following secular determinant within a Hückel-like approximation (Supporting Information):

$$\begin{vmatrix} E_d - E_\Phi & 0 & H \\ 0 & E_d - E_\Phi & H \\ H & H & E_{nb} - E_\Phi \end{vmatrix} = 0$$

i.e.,

$$(E_d - E_\Phi)[(E_d - E_\Phi)(E_{nb} - E_\Phi) - 2H^2] = 0$$

leading to

$$E_\Phi(r) = \frac{E_d(r) + E_{nb}(r) - \sqrt{[E_d(r) - E_{nb}(r)]^2 + 8[H(r)]^2}}{2} \quad (1)$$

Then, the energy profile of the adiabatic ground state is obtained through the mixing with the bonding state as it appears in the following secular determinant:

$$\begin{vmatrix} E_b - E_\psi & H' \\ H' & E_\Phi - E_\psi \end{vmatrix} = 0$$

where H' is the resonance energy between the repulsive state and the bonding state. This leads to

$$E_\psi(r) = \frac{E_b(r) + E_\Phi(r) - \sqrt{[E_b(r) - E_\Phi(r)]^2 + 4[H'(r)]^2}}{2} \quad (2)$$

We now have to specify $E_b(r)$, $E_d(r)$, $E_{nb}(r)$, $H(r)$, and $H'(r)$. The bonding-state diabatic profile, $E_b(r)$, is given by the following Morse curve (Figure 4d)

$$E_b(r) = (2E^{\text{rad}}_b - E_{\text{dim}})\{1 - \exp[-\beta(r - r_0)]\}^2 + E_{\text{dim}} \quad (3)$$

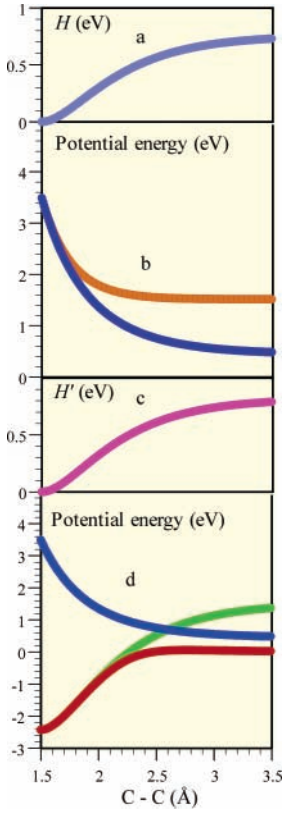

Figure 4. Dimerization of allyl radicals. (a) Variation of the resonance energy H with the carbon−carbon distance. (b) Potential energy profiles of repulsive states. (Orange) nonbonding state and dual states. (Blue) repulsive state after mixing. (c) Variation of the resonance energy H' with the carbon−carbon distance. (d) Potential energy profiles for (blue) repulsive state, (green) bonding state, and (red) adiabatic states ground state.

SCHEME 1

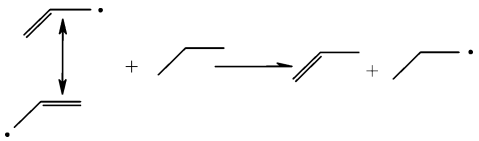

where E^{rad}_b is the energy of the radical in the bonding state, E_{dim} is the energy of the dimer, r_0 is the equilibrium C−C distance in the dimer, and β is a shape factor defined as

$$\beta = \sqrt{\frac{f}{2(2E^{\text{rad}}_b - E_{\text{dim}})}} \quad (4)$$

where f is the bond force constant.

In the case of allyl radicals, B3LYP/6-31G* geometry optimization allowed the determination of r_0 (1.5 Å), of $E_{\text{dim}} = -2.43$ eV, of the force constant and thus β (2 Å^{-1}, according to eq 4, using the value of E^{rad}_b determined below). The later value is referred to the energy of the diabatic potential energy curve at infinite distance, taken as the origin (i.e., twice the actual energy of the allyl radical), which was derived from a UB3LYP/6-31G* calculation. E^{rad}_b, which is defined as the difference between the energies of the localized allyl radical and the actual allyl radical (see top of Figure 2), can be approximated by Benson's stabilization energy[2b,9] drawn from the difference between the strength of the C−H bonds in propane and propene (Scheme 1).

Simple valence bond theory predicts that the repulsion between the two bonds is approximatively equal to one-half of

the bonding energy.[10] The profile, $E_{nb}(r)$, may therefore be represented by the following function of the C−C distance (Figure 4b):

$$E_{nb} = \left(E_b^{\mathrm{rad}} - \frac{E_{\mathrm{dim}}}{2}\right)\{\exp[-\beta(r - r_0)]\}^2 + 2E_{nb}^{\mathrm{rad}} \quad (5)$$

In the particular case of the dimerization of two allyl radicals,

$$E_{nb}^{\mathrm{rad}} = E_b^{\mathrm{rad}}$$

because only two mesomeric forms of equal energy are involved. Simple valence bond theory also predicts that both dual states are exactly as much repulsive as the nonbonding state thanks to the fact that in the dual-state case there is a three-electron repulsion between an unpaired electron and a bond whereas in the nonbonding state there is a repulsion between two bonds.[10] Assuming that the dual states are purely repulsive leads to (Figure 4b)

$$E_d(r) = \left(E_b^{\mathrm{rad}} - \frac{E_{\mathrm{dim}}}{2}\right)\{\exp[-\beta(r - r_0)]\}^2 + E_b^{\mathrm{rad}} + E_{nb}^{\mathrm{rad}} \quad (6)$$

As seen in Figure 3, H vanishes at short distance, becoming nil for $r = r_0$ and becoming maximal for $r \rightarrow \infty$, paralleling the cleavage of the bond between these two extremes.

We thus propose to model the variation of H by a Morse curve having the same shape as the Morse curve representing the energy of the bonding state:

$$\frac{H_{r=\infty} - H(r)}{H_{r=\infty}} = \frac{E_{b,r=\infty} - E_b(r)}{(2E_b^{\mathrm{rad}} - E_{\mathrm{dim}})} = 1 - \{1 - \exp[-\beta(r - r_0)]\}^2$$

i.e.,

$$H(r) = H_{r=\infty}\{1 - \exp[-\beta(r - r_0)]\}^2 \quad (7)$$

with

$$H_{r=\infty} = E_b^{\mathrm{rad}} \quad (8)$$

in the particular case of the dimerization of two allyl radicals.

For the same reasons, the variation of H' is

$$H'(r) = H'_{r=\infty}\{1 - \exp[-\beta(r - r_0)]\}^2 \quad (9)$$

The value of H' at infinite distance, $H'_{r=\infty}$, is given by

$$H'_{r=\infty} = \sqrt{E_b^{\infty} E_{\Phi}^{\infty}} \quad (10)$$

which results from the resolution of eq 2 with the condition

$$E_{\psi}(r = \infty) = 0$$

Because

$$E_{\phi}^{\infty} = \frac{E_b^{\mathrm{rad}} + 3E_{nb}^{\mathrm{rad}} - \sqrt{[E_b^{\mathrm{rad}} - E_{nb}^{\mathrm{rad}}]^2 + 8[H_{r=\infty}]^2}}{2}$$

and $E_b^{\infty} = 2E_b^{\mathrm{rad}}$, in the particular case of the dimerization of two allyl radicals, where $E_{nb}^{\mathrm{rad}} = E_b^{\mathrm{rad}}$ and $H_{r=\infty} = E_b^{\mathrm{rad}}$,

$$H'_{r=\infty} = \sqrt{2E_b^{\mathrm{rad}}(2E_b^{\mathrm{rad}} - \sqrt{2}H_{r=\infty})} = 2\sqrt{1 - \frac{1}{\sqrt{2}}}E_b^{\mathrm{rad}} \quad (11)$$

The values of all parameters are summarized in Table 1.

The H profile is shown in Figure 4a; the nonbonding, dual energy profiles are displayed in Figure 4b; the adiabatic ground-state energy profile and the bonding and repulsive energy profiles are displayed in Figure 4d; and the mixing resonance energy H' is displayed in Figure 4c. We see that the adiabatic ground-state potential energy profile does not exhibit any significant maximum. This result, which will be validated below by means of a full quantum chemical calculation, implies the absence of activation barrier for the coupling of two allyl radicals, just as with simple methyl radicals.

To check the reliability of this two-state description, we carried out the full four-state description. The mixing of the four valence bond states $|b\rangle$, $|d\rangle$, $|d'\rangle$, and $|nb\rangle$ is obtained through the following secular determinant (Supporting Information):

$$\begin{vmatrix} E_b - E_{\psi} & H & H & 0 \\ H & E_d - E_{\psi} & 0 & H \\ H & 0 & E_d - E_{\psi} & H \\ 0 & H & H & E_{nb} - E_{\psi} \end{vmatrix} = 0$$

In other words,

$$(E_d - E_{\psi})\left[(E_b - E_{\psi})(E_d - E_{\psi})(E_{nb} - E_{\psi}) - 4H^2\left(\frac{E_b + E_{nb}}{2} - E_{\psi}\right)\right] = 0 \quad (12)$$

The adiabatic ground-state energy E_{ψ} is the more negative solution of eq 12. The specification of $E_b(r)$, $E_d(r)$, $E_{nb}(r)$, and $H(r)$ is the same as previously developed (eqs 3, 5, 6, and 7). Numerical resolution of eq 12 has been performed and leads to an adiabatic ground-state energy profile very close to the one obtained from the two-state model (Figure 5).

A further validation of the two-state model will be presented in the next section through comparison with DFT calculations. The advantage of the simplified two-state model over a more complete valence bond model clearly appears here. Even for a very simple system, the valence bond model requires taking into account at least four valence bond states and leads to a nonanalytical solution for the ground-state energy, whereas the two-state model leads to an approximation of the adiabatic ground-state energy with analytical expressions (eqs 1−11),[11] thus allowing the prediction of the height of the barrier, if any, using only information relative to reactants and products.

Although interesting, thanks to its simplicity in explaining the model, the case of allyl radicals is not the best choice to demonstrate the formation of an activation barrier and thus to analyze its origin. This is the reason that we apply now the model to the case of benzyl radicals. The main change from the preceding case is the fact that four mesomeric forms (Scheme 2) are now involved instead of two. A valence bond description would thus require us to take into account 16 states with 1 bonding state and 15 repulsive states involving either a radical−bond repulsion or a bond−bond repulsion. Building the repulsive more stable state Φ_{rep} was performed in two steps. We first consider all mesomeric forms with the unpaired electron not localized on the dimerizing carbon as a single nonbonding radical form with an energy E_{nb}^{rad}. The 15 repulsive interactions are thus replaced by 3 interactions described by a nonbonding

TABLE 1: Parameters for the Construction of the Potential Energy Profiles in Figures 4 and 7

		benzyl	
radical	allyl	7,7′	4,4′
r_0 (Å)[a]	1.5	1.6	1.6
f (eV/Å^{-2})[a]	31.5	21.6	23.3
β (Å^{-1})[b]	2.00	1.67	1.84
E_{dim}(eV)[a]	−2.43	−2.70	0.113
E_b^{rad} (eV)[c]	0.757	0.584	1.77
s_b[d]	0.50	0.50	0.18
E_{nb}^{rad} (eV)[e]	0.757	0.584	0.388
$H_{r=\infty}$ (eV)	0.757[f]	0.584[g]	0.807[g]
$H'_{r=\infty}$ (eV)	0.819[h]	0.632[i]	0.615[i]

[a] From B3LYP/6-31G* geometry optimization of the dimer. [b] From eq 4. [c] See Schemes 1 and 3. [d] From UB3LYP/6-31G* geometry optimization of the radical. [e] From eq 15. [f] From eq 8. [g] From eq 13. [h] From eq 11. [i] From eq 14.

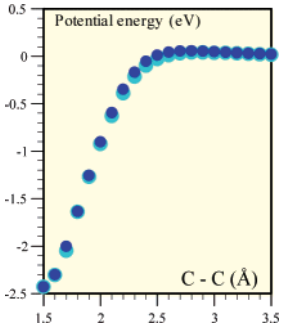

Figure 5. Dimerization of allyl radicals. Comparison of the two-state model predicted (light blue) and the four valence bond states model (dark blue) adiabatic potential energy profiles.

SCHEME 2

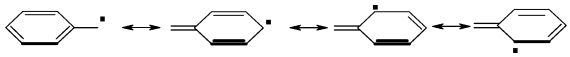

state and 2 dual states as depicted in Figure 6 for the 7,7′ and 4,4′ dimerization together with the bonding state. The second step consists of mixing the three repulsive states as explained for the allyl model (eq 1) to obtain the repulsive state of interest Φ_{rep}. This state is then mixed with the bonding state in the framework of the two-state model (eqs 2−7, 9, and 10). Equation 8 is replaced by

$$H_{r=\infty} = \sqrt{E_b^{rad} E_{nb}^{rad}} \tag{13}$$

Because

$$E_\Phi^\infty = \frac{E_b^{rad} + 3E_{nb}^{rad} - \sqrt{[E_b^{rad} - E_{nb}^{rad}]^2 + 8E_b^{rad} E_{nb}^{rad}}}{2}$$

and $E_b^\infty = 2E_b^{rad}$, equation 11 is replaced by

$$H'_{r=\infty} = \sqrt{E_b^{rad}(E_b^{rad} + 3E_{nb}^{rad} - \sqrt{[E_b^{rad} - E_{nb}^{rad}]^2 + 8E_b^{rad} E_{nb}^{rad}})} \tag{14}$$

The determination of the various ingredients of the model is as follows. (They are listed in Table 1.) E_b^{rad} was again obtained from the stabilization energy corresponding to the two reactions depicted in Scheme 3 for the 7,7′ and 4,4′ dimerization, successively. The energy of the actual benzyl radical, which serves as the origin for the energy scale, is derived from a UB3LYP/6-31G* calculation as before. The diabatic energy

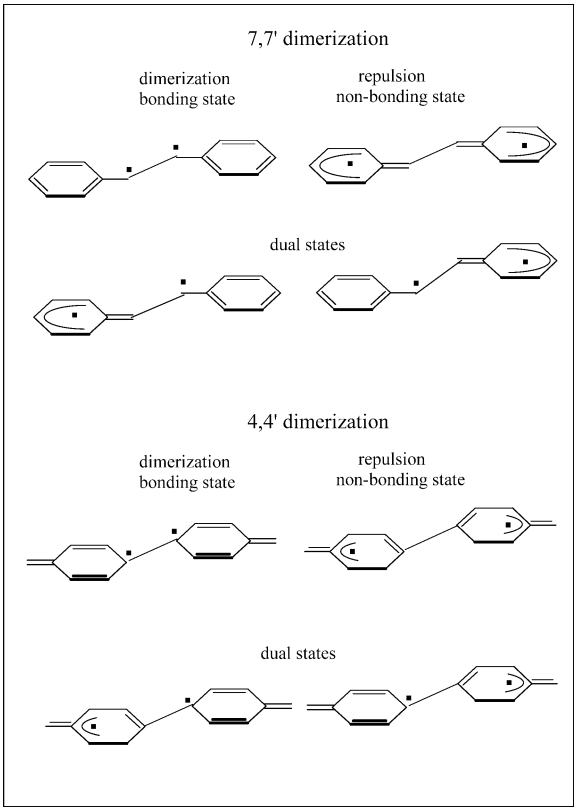

Figure 6. 7,7′ and 4,4′ dimerization of benzyl radicals. Bonding, nonbonding, and dual states.

SCHEME 3

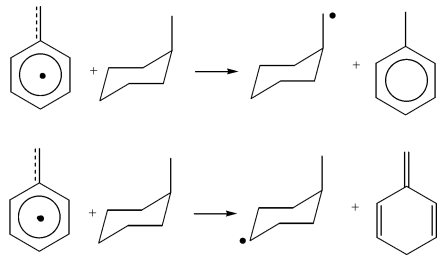

profile of the bonding state is obtained from eq 3, where E_{dim} and β (Table 1) are obtained from a B3LYP/6-31G* geometry optimization of the dimer as in the allyl case. Geometry optimization of the actual benzyl radical also provided the spin densities, s_b, at each carbon from which the energy of the nonbonding state could be derived according to eq 15:

$$E_{nb}^{rad} = E_b^{rad}\frac{s_b}{1 - s_b} \tag{15}$$

The carbon spin densities of interest are derived from the Mulliken population analysis by taking into account only the spin densities on carbon atoms having an excess of spin up.

The values of all parameters are summarized in Table 1, leading to the potential energy profiles shown in Figure 7 for the 7,7′ and 4,4′ dimerization. The characteristics of dimerization at the 7 position (i.e., at the extra-ring carbon) are very similar to those of the allyl radicals, showing no significant activation barrier. On the contrary, dimerization at the 4 position shows a quite sizable activation barrier. The existence of the barrier is related to the relatively poor unpaired electron density at the 4 carbon. A substantial amount of energy is thus required to bring the unpaired electron to the position appropriate for dimerization

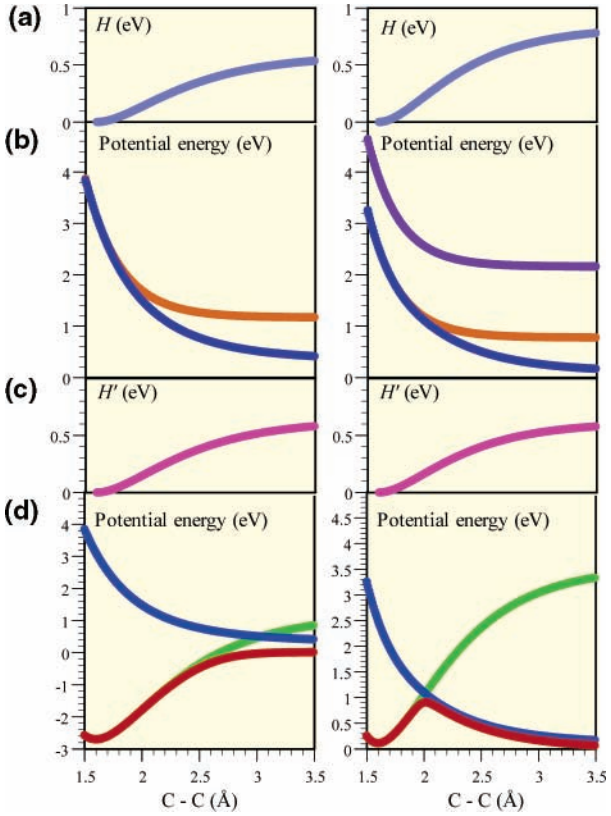

Figure 7. 7,7′ (left) and 4,4′ (right) dimerization of benzyl radicals. (a) Variation of the resonance energy H with the carbon−carbon distance. (b) Potential energy profiles of repulsive states. (Purple) nonbonding state and (orange) dual states. (Blue) repulsive state after mixing. (c) Variation of the resonance energy H' with the carbon−carbon distance. (d) Potential energy profiles of the (blue) repulsive state, (green) bonding state, and (red) adiabatic ground state.

to take place. Localization of the unpaired electron means that the relative weight of the bonding state Φ_b with respect to the repulsive state Φ_{rep} in the wave function ψ increases. Because the bonding state has a higher energy than the repulsive state at large bond distances, increasing its weight in the adiabatic ground states generates an increase of the corresponding energy, thus leading to an activation barrier. For the same reasons, the driving force for dimerization is much smaller (practically zero) than in the 7,7′ case. This example clearly shows that the two-state model is helpful in deciphering the origin of the activation barrier with only the help of information relative to reactants and products. This is particularly interesting for systems where full quantum chemical calculations are time-consuming.

Validation and Applications of the Model

Figure 8 compares the adiabatic potential energy profiles derived from the model to the curves obtained directly by UB3LYP/6-31G* computation for the three dimerization reactions dealt with in the previous section.[12] The agreement between the two curves is quite satisfactory, especially in view of the approximate character of several assumptions. We also checked that, in the case of 4,4′ benzyl dimerization, the transition state and the intrinsic reaction coordinate pathways from transition state to reactants and products agree with the potential energy profile just calculated (Figure 8).

Concerning benzyl radicals, the above analysis, leading to the results represented in Figure 8, shows that 7,7′ dimerization is much more favorable than 4,4′ dimerization, not only because the driving force is much higher in the first case than in the second but also because there is no activation barrier for the

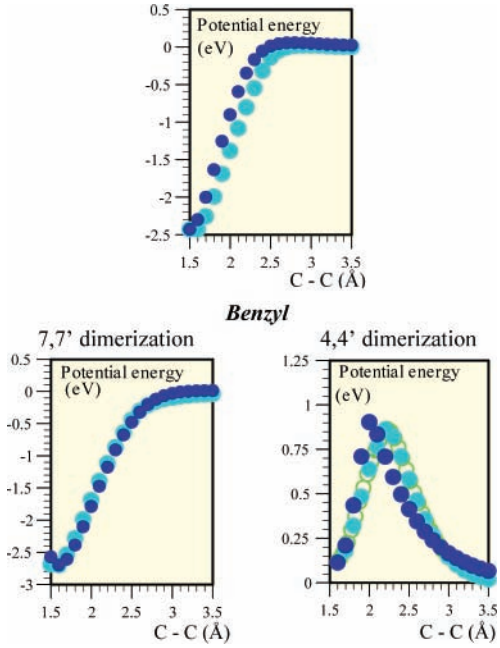

Figure 8. Validation of the model by comparing the model predicted (dark blue) and the UB3LYP/6-31G* calculated (light blue) adiabatic potential energy profiles for the three indicated dimerizations. (Green ○): transition state and intrinsic reaction coordinate pathway.

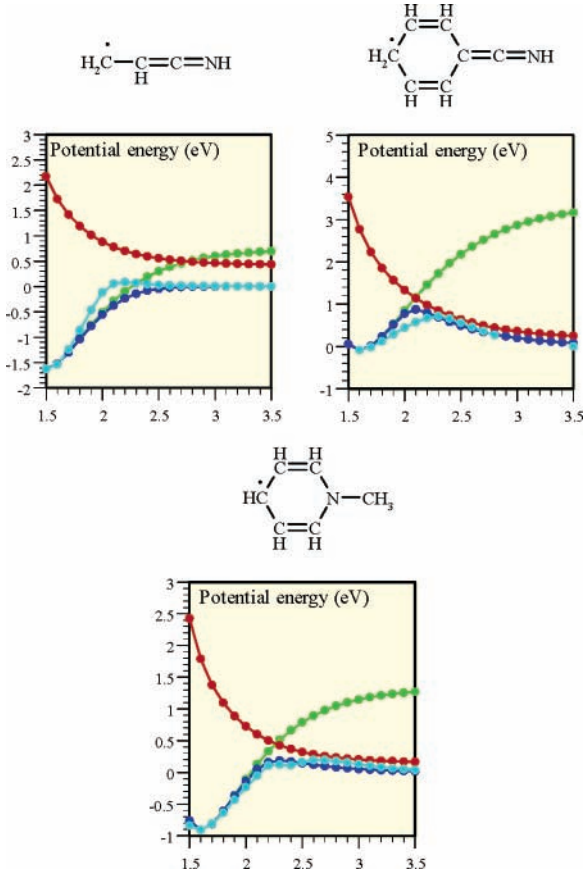

Figure 9. Dimerization of protonated nitrile anion radicals and of an analogue of NAD: (green), bonding state; (red), repulsive states; (dark blue, light blue) model predicted and UB3LYP/6-31G* calculated adiabatic profiles, respectively.

7,7′ reaction whereas the 4,4′ coupling is hampered by a large activation barrier.

Other examples are displayed in Figure 9. The first are related to the investigation of anion radicals of conjugated nitriles,

TABLE 2: Parameters for the Construction of the Potential Energy Profiles in Figure 9

radical	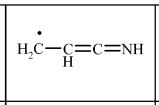	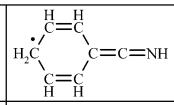	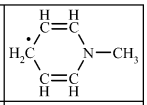
r_0 (Å) [a]	1.5	1.6	1.6
f(eV/Å^{-2}) [a]	25.7	23.4	23.15
β(Å^{-1}) [b]	2.33	1.84	2.275
E_{dim} (eV) [a]	-1.627	-0.088	-0.908
E_b^{rad} (eV)	0.37	1.687	0.664
s_b [c]	0.625	0.235	0.335
E_{nb}^{rad} (eV) [e]	0.617	0.518	0.334
$H_{r=\infty}$ (eV)	0.478 [f]	0.935 [g]	0.471 [g]
$H'_{r=\infty}$ (eV)	0.560 [h]	0.769 [i]	0.441 [i]

[a] From B3LYP/6-31G* geometry optimization of the dimer. [b] From eq 4. [c] From UB3LYP/6-31G* geometry optimization of the radical. [e] From eq 15. [f] From eq 8. [g] From eq 13. [h] From eq 11. [i] From eq 14.

SCHEME 4

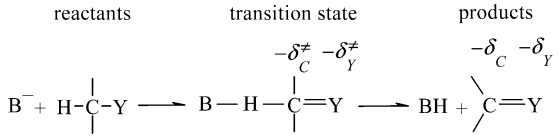

where comparison with their protonated counterpart is a precious clue in the discussion. [4] The values of the parameters used to construct the diagrams of Figure 9 are summarized in Table 2. The radical derived from acrylonitrile shows practically no activation barrier, whereas the radical derived from benzonitrile exhibits a significant barrier and practically no driving force for dimerization. The last example shown in Figure 9 is a synthetic analogue of the NAD radical. Its dimerization is endowed with a small but distinct activation barrier, in line with the observation that the dimerization of similar radicals is below the diffusion limit.[13]

We note, for these three radicals too, the good agreement between the application of the model and the direct UB3LYP/6-31G* computation of the adiabatic potential energy profile.

Nonperfect Synchronization of Bond Cleavage and Electron Delocalization?

The deprotonation of carbon acids bearing groups on which the developing charge may be delocalized (usually electron-withdrawing groups connected to the reacting carbon either directly or through an unsaturated hydrocarbon structure) has provided the main experimental basis for the principle of nonperfect synchronization (PNS).[8,14,15] In such reactions, two molecular processes, here deprotonation and delocalization of charges, are deemed to have made unequal progress at the transition state, which therefore possesses an imbalanced character.

The imbalanced character of the transition state for this family of reactions is defined according to the distribution of charge over the reaction carbon and the adjacent group, Y, as shown in Scheme 4.

Imbalance is expressed by

$$\frac{\delta_C^{\neq}}{\delta_Y^{\neq}} > \frac{\delta_C}{\delta_Y}$$

with $\delta_C + \delta_Y = 1$ (i.e., the negative charge is less resonance

SCHEME 5

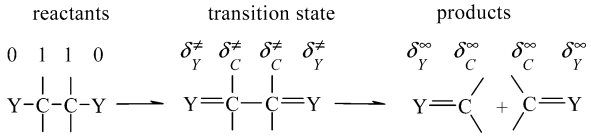

delocalized over the Y group in the transition state than it is in the product state). The reasons that the transition states of these deprotonation reactions are imbalanced have been the object of many investigations and debates.[8,14−16] The resolution of this problem, and more generally the understanding of the dynamics of proton exchange at carbon atoms, is complicated by the necessity of taking into account both homolytic and ionic states.[17] In addition, proton tunneling is likely to play a prominent role in these reactions.[18]

In contrast, the dimerization of conjugated radicals, as discussed above, appears to be a particularly simple case where the PNS could be tested. The adiabatic ground-state wave function is written as $\psi = c_b\Phi_b + c_{rep}\Phi_{rep}$, where Φ_b represents a bonding state with an unpaired electron fully localized on the dimerizing carbons, whereas Φ_{rep} represents all other valence bond structures where at least one unpaired electron is not localized on a dimerizing carbon. Thus, $\epsilon = (c_b/c_{rep})^2$ is an index to the degree of delocalization (Scheme 5): the more delocalized the structure, the smaller ϵ.[19]

$$\frac{\delta_C}{\delta_Y} = \epsilon$$

Imbalance is then expressed by

$$\epsilon_\infty < \epsilon^{\ddagger}$$

(i.e., the unpaired electron is less delocalized over the Y group in the transition state than it is in the product state). Starting from the dimer, Figure 10 shows that for the allyl and 4,4′ benzyl dimers (taken as example of dimerization without and with activation barrier) the cleavage of the bond, designated as the main process, is accompanied by resonance delocalization of each electron of the σ-bond over the rest of each moiety as the bond stretches. It is clear that the degree of delocalization increases from reactant to products (i.e., there is a decrease of ϵ). It is much less in the transition state, when there is a transition state, than in each of the two radicals. In this sense, delocalization lags behind bond breaking, thus apparently providing another example of the application of the PNS. But there is, in fact, no way that the degree of delocalization should be the same

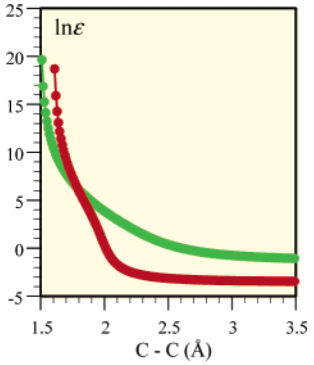

Figure 10. Variation of ln ϵ with the carbon−carbon distance in the dimerization of the allyl radical (green line) and the benzyl radical at position 4 (red line).

over the whole reaction profile, taking at once the value that it will have when radical formation reaches completeness. This remark applies whether dimerization is endowed with an activation barrier. It follows that the simple invocation of the PNS is not sufficient to explain whether an activation barrier exists or does not exist. It is actually necessary to specify how the degree of delocalization varies with the degree of bond cleavage. The present model assumes that resonance, as measured by the exchange energy H', increases regularly at the same pace as bond cleavage, allowing delocalization to take place progressively. A comparison with quantum chemical calculation validates the model and therefore validates the assumption. In this sense, delocalization is synchronous with bond breaking.

Concluding Remarks

1. Localization of the unpaired electron on the dimerizing carbon upon bond formation is an essential factor of both the thermodynamics and kinetics of unsaturated radical dimerizations.

2. From this starting point, a model of the dimerization/cleavage reaction may be built on the basis of the resonance combination of two states, one in which each electron of the forming bond is localized on the dimerizing carbon atom and another that is purely repulsive, built up from valence bond structures in which there are only repulsive interactions between mesomeric forms of each radical. The ground-state potential energy profiles thus predicted are in satisfactory agreement with the profiles generated by quantum chemical calculations. According to the nature of the radicals, the reactions profiles may or may not exhibit an activation barrier to dimerization

3. The two-state model thus helps us to understand the origin of the activation barrier. The crucial factor in this connection is the magnitude of the localization energy (i.e., the resonance energy H). A large value of this parameter results in a decrease of both the driving force and the appearance and an increase of the activation barrier.

4. The model allows the prediction of the existence and approximate height of the activation barrier from data pertaining only to the reactant and product systems. This is particularly interesting for systems where full quantum chemical calculations are time-consuming.

5. The dimerization of unsaturated radicals appears to be a particularly illuminating example where an accompanying process, namely, resonance stabilization of the forming radical, lags behind the main process (i.e., bond formation). From an alternative viewpoint, the observation that the validation of the assumption that the resonance integral increases at the same pace as bond cleavage leads to the conclusion that delocalization synchronously accompanies bond breaking.

Supporting Information Available: Rumer functions for the allyl radical. Establishment of the secular determinant for the determination of the repulsive state. Establishment of the secular determinant for the four valence bond state treatment. Methodology for quantum chemical calculations. This material is available free of charge via the Internet at http://pubs.acs.org.

References and Notes

(1) Griller, D.; Ingold, K. U. *Acc. Chem. Res.* **1976**, *9*, 13.

(2) (a) Kerr, J. A. *Chem. Rev.* **1966**, *66*, 465. (b) O'Neal, H. E.; Benson, S. W. Thermochemistry of Free Radicals. In *Free Radicals*; Kochi, J. K., Ed.; Wiley: New York, 1973; Vol. 2, pp 291−302.

(3) (a) Maslak, P.; Narvaez, J. N. *Angew. Chem., Int. Ed. Engl.* **1990**, *29*, 283. (b) Laarhoven, L. J. J.; Born, J. G. P.; Arends, I. W. C. E.; Mulder, P. *J. Chem. Soc., Perkin Trans. 2* **1997**, 2307.

(4) Costentin, C.; Savéant, J.-M. *J. Electroanal. Chem.* **2004**, *564*, 99.

(5) (a) One example is the NAD radical and closely related radicals, whose dimerization is well below the diffusion limit (ca. 10^6 M^{-1} s^{-1}). (b) Schmakel, C. O.; Santhanam, K. S. V.; Elving P. J. *J. Am. Chem. Soc.* **1975**, *97*, 5083. (c) Jensen, M. A.; Elving P. J. *Biophys. Biochim. Acta* **1984**, *764*, 310.

(6) (a) Another interesting example is found with nitrogen-centered radicals, namely, the two substituted aminyl radicals $\bullet N(OH)_2$ and $\bullet N(NH2)_2$. (b) Leroy, G.; Sana, M. *THEOCHEM* **1988**, *179*, 237. (c) Sana, M.; Leroy, G.; Vinson, L. K.; Dannenberg, J. J. *THEOCHEM* **1989**, *205*, 89. (d) See also *Substituent Effects in Radical Chemistry*; Viehe, H. G., Janousek, Z., Merényi, R., Eds.; NATO ASI Series; D. Reidel: Dordrecht, The Netherlands, 1986; Vol. 189, pp 162−163.

(7) Ingold, K. U. Rate Constants for Free Radical Reactions. In *Free Radicals*; Kochi, J. K., Ed.; Wiley: New York, 1973; Vol. 1, pp 40−66.

(8) (a) See refs 8b and c and references therein. (b) Bernasconi, C. F. *Adv. Phys. Org. Chem.* **1992**, *27*, 119. (c) Costentin, C.; Savéant, J.-M. *J. Am. Chem. Soc.* **2004** *126*, 14787.

(9) (a) Benson, S. W. *Thermochemical Kinetics*; Wiley: New York, 1968. (b) Golden, D. M.; Benson, S. W. *Chem. Rev.* **1969**, *69*, 125.

(10) Shaik, S.; Hiberty, P. C. Valence Bond Mixing and Curve Crossing Diagrams in Chemical Reactivity and Bonding. In *Advances in Quantum Chemistry*; Academic Press: New York, 1995; Vol 26, pp 99−163.

(11) This is even truer with radicals described with n mesomeric forms where a valence bond model would require the consideration of n^2 valence bond states. However, this argument remains true with the two-state model where building up of the repulsive state then requires the mixing of $n^2 - 1$ states. The treatment of benzyl radical dimerization shows us how to deal with this issue.

(12) (a) Because we are not looking for a very accurate determination of the small activation energy, this level of calculation is sufficient for testing the model. We note in this connection that it is able to reproduce satisfactorily the experimental values of C−C bond dissociation energies. For example, the bond dissociation energy of ethane is reproduced with an accuracy better than 1%. (b) Feng, Y.; Liu, L.; Wang, J.-T.; Huang, H., Guo, Q.-X. *J. Chem. Inf. Comput. Sci.* **2003**, *43*, 2005.

(13) Anne, A.; Hapiot, P.; Moiroux, J.; Savéant, J.-M. *J. Electroanal. Chem.* **1992**, *331*, 959.

(14) (a) Kresge, A. J. *Chem. Soc. Rev.* **1973**, *2*, 475. (b) Kresge, A. J. *Can. J. Chem.* **1974**, *52*, 1897

(15) (a) Bernasconi, C. F. *Acc. Chem. Res.* **1987**, *20*, 301. (b) Bernasconi, C. F. *Acc. Chem. Res.* **1992**, *25*, 9. (c) Albery, W. J.; Bernasconi, C. F.; Kresge, A. J. *J. Phys. Org. Chem.* **1988**, *1*, 29

(16) Hine, J. *Adv. Phys. Org.* **1977**, *15*, 1.

(17) (a) The role of the homolytic states appears to be particularly important in the deprotonation of cation radicals, as shown in the case of NADH analogues. (b) Anne, A.; Fraoua, S.; Grass, V.; Moiroux, J.; Savéant, J.-M. *J. Am. Chem. Soc.* **1998**, *120*, 2951.

(18) (a) Borgis, D.; Hynes, J. T. *J. Phys. Chem.* **1996**, *100*, 1118. (b) Borgis, D.; Hynes, J. T. *J. Chem. Phys.* **1993**, *170*, 891. (c) Borgis, D.; Lee, S.; Hynes, J. T. *Chem. Phys. Lett.* **1989**, *162*, 19. (d) Lee, S.; Hynes, J. T. *J. Chim. Phys.* **1996**, *93*, 1783.

(19) Within the framework of the simplified model developped here, $\epsilon = (c_b/c_{rep})^2 = [H'/(E_b - E_\psi)]^2$.